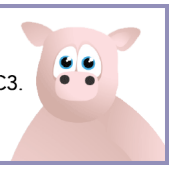

The Journal of Immunology

Clonally Diverse T Cell Homeostasis Is Maintained by a Common Program of Cell-Cycle Control

Thea Hogan, Andrey Shuvaev, Daniel Commenges, Andrew Yates, Robin Callard, Rodolphe Thiebaut and Benedict Seddon

J Immunol 2013; 190:3985-3993; Prepublished online 8 March 2013;
doi: 10.4049/jimmunol.1203213
http://www.jimmunol.org/content/190/8/3985

The Journal of Immunology is published twice each month by
The American Association of Immunologists, Inc.,
9650 Rockville Pike, Bethesda, MD 20814-3994.

Print ISSN: 0022-1767 Online ISSN: 1550-6606.

Clonally Diverse T Cell Homeostasis Is Maintained by a Common Program of Cell-Cycle Control

Thea Hogan,*[,1,2] Andrey Shuvaev,[†,1,3] Daniel Commenges,[†] Andrew Yates,[‡] Robin Callard,* Rodolphe Thiebaut,[†,4] and Benedict Seddon[§,4]

Lymphopenia induces T cells to undergo cell divisions as part of a homeostatic response mechanism. The clonal response to lymphopenia is extremely diverse, and it is unknown whether this heterogeneity represents distinct mechanisms of cell-cycle control or whether a common mechanism can account for the diversity. We addressed this question by combining in vivo and mathematical modeling of lymphopenia-induced proliferation (LIP) of two distinct T cell clonotypes. OT-I T cells undergo rapid LIP accompanied by differentiation that superficially resembles Ag-induced proliferation, whereas F5 T cells divide slowly and remain naive. Both F5 and OT-I LIP responses were most accurately described by a single stochastic division model where the rate of cell division was exponentially decreased with increasing cell numbers. The model successfully identified key biological parameters of the response and accurately predicted the homeostatic set point of each clone. Significantly, the model was successful in predicting interclonal competition between OT-I and F5 T cells, consistent with competition for the same resource(s) required for homeostatic proliferation. Our results show that diverse and heterogenous clonal T cell responses can be accounted for by a single common model of homeostasis. ***The Journal of Immunology*****, 2013, 190: 3985–3993.**

The size and composition of the T lymphocyte compartment is subject to strict homeostatic regulation and is remarkably stable throughout life, despite variable dynamics in cell production and death during T cell development and immune responses (1, 2). Homeostasis is achieved by careful orchestration of lymphocyte survival and cell division. Naive T cell survival critically depends on sufficient access to the cytokine IL-7 (3–6) and TCR signals (7–12) induced by contact with self-peptide MHC (spMHC) on dendritic cells (13). Lymphopenia induces naive T cells to undergo cell divisions that depend on TCR signaling (3, 14–17), but differ from Ag-induced proliferation by the nonredundant requirement for IL-7 (4, 6, 13). Interestingly, lymphopenia-induced homeostatic proliferation can also be associated with acquisition of a memory phenotype, and such cells share both functional and molecular characteristics of conventional memory cells (18, 19). In lymphoreplete mice, naive T cells are largely noncycling (20). In contrast, homeostatic cell division plays a more important role in maintaining naive T cell homeostasis in humans, even in replete conditions, as cell division is evident in the naive pool (21, 22), whereas recent thymic emigrants and naive T cells from cord blood have an enhanced ability to divide in response to IL-7 signaling (23, 24).

To date, our understanding of the processes controlling survival and proliferation of T cells is largely qualitative. Detailed quantitative knowledge of how homeostatic responses result in the observed equilibrium of the T cell pool with a given size and composition is lacking. The homeostatic T cell response to lymphopenia results in highly diverse cellular behavior by different T cell subsets and clonotypes. Some T cell clonotypes hardly respond at all, whereas others undergo multiple rounds of cell division and phenotypic differentiation (25–28). The question remains, however, whether the diverse homeostatic cell division observed in vivo can be accounted for by a single set of simple rules, and if so, which are the key parameters that explain the diverse range of behavior? Furthermore, can such a set of rules be successfully extrapolated to make specific predictions of complex cellular behavior such as competition between clonotypes for a common resource? In this study, we sought to address these questions by using mathematical models based on current knowledge of cell-cycle regulation.

Materials and Methods

Mice

C57BL/6J Ly5.1, C57BL/6J *Rag1*$^{-/-}$, F5 *Rag1*$^{-/-}$ (F5), and OT-I *Rag1*$^{-/-}$ (OT-I) mice (all H-2^{b} haplotype) were maintained in a conventional

*Institute of Child Health, University College London, London, WC1N 1EH, United Kingdom; [†]INSERM U897, Institut de Santé Publique, d'Épidémiologie et de Développement, Université Bordeaux Segalen, Bordeaux 33076, France; [‡]Albert Einstein College of Medicine, Bronx, NY10461; [§]Division of Immune Cell Biology, Medical Research Council National Institute for Medical Research, London, NW7 1AA, United Kingdom

[1]T.H. and A.S. contributed equally to this work.

[2]Current address: Division of Immune Cell Biology, Medical Research Council National Institute for Medical Research, London, United Kingdom.

[3]Current address: Institute of Fundamental Preparation, Siberian Federal University, Krasnoyarsk, Russia.

[4]R.T. and B.S. contributed equally to this work.

Received for publication November 21, 2012. Accepted for publication February 5, 2013.

This work was supported by the Biotechnology and Biological Sciences Council, U.K., and the Agence Nationale de la Recherche, France (ANR-BBSRC-SysBio 07BSYS007).

Address correspondence and reprint requests to Rodolphe Thiebaut or Dr. Benedict Seddon, INSERM U897, Institut de Santé Publique, d'Épidémiologie et de Développement Université Bordeaux Segalen, Bordeaux 33076, France (R.T.) or Division of Immune Cell Biology, Medical Research Council National Institute for Medical Research, Mill Hill, London, NW7 1AA, United Kingdom (B.S.). E-mail addresses: rodolphe.thiebaut@isped.u-bordeaux2.fr (R.T.) or bseddon@nimr.mrc.ac.uk (B.S.)

The online version of this article contains supplemental material.

Abbreviations used in this article: 7AAD, 7 aminoactinomycin D; CrV, comparison reference value; CTV, CellTrace Violet; LIP, lymphopenia-induced proliferation; SM, Smith and Martin; spMHC, self-peptide MHC; SSD, single stochastic division; SSR, sum of squared residuals.

pathogen-free colony at the National Institute for Medical Research (London, U.K.). All experiments were performed according to institutional guidelines and Home Office regulations.

Flow cytometry

Flow cytometry was conducted on 2–5 $\times$ 10^6 lymph node or spleen cells, or 40 μl whole blood. Cells were incubated for 1 h at 4°C with saturating concentrations of Abs and fixed with either intracellular fixation buffer (eBioscience) or Fix/Perm (eBioscience). For intracellular staining, fixed cells were incubated with saturating concentrations of Ab for 1 h at room temperature. DNA staining was performed by addition of 0.25 μg/ml 7 aminoactinomycin D (7AAD; Sigma) immediately before sample acquisition. mAbs used in this study were as follows: allophycocyanin-CD8 (53-6.7; eBioscience), allophycocyanin-eFluor 780-CD44 (IM7; eBioscience), eFluor 450-CD5 (53-7.3; eBioscience), FITC-CD5 (53-7.3; eBioscience), Pacific Orange-CD8 (5H10; Invitrogen), PE-Ly5.2 (104; eBioscience), and PE-Ki67 (B56, BD Pharmingen). Multicolor acquisition was performed on a Canto-II instrument (BD Biosciences), and data analysis was performed using FlowJo version 9.3 software (Tree Star).

Labeling and adoptive transfer of T cells

Single-cell suspensions were prepared from the lymph nodes of OT-I or F5 donor mice. Cells were labeled with 2 μM of either CFSE (Invitrogen) or CellTrace Violet (CTV) (Invitrogen) in Dulbecco's PBS (Invitrogen) for 10 min at 37°C and washed twice. One to two million labeled lymphocytes were transferred to recipient mice by i.v. injection.

Calculations of cell recovery and expansion

Cell counts from spleens and lymph nodes of recipient mice were determined using a Scharf Instruments Casy Counter, and the proportion of total cells that was donor derived was determined by flow cytometry. Total donor cell recovery for individual mice was calculated by summing the number of donor cells recovered from the spleen and lymph nodes. The size of the precursor population was calculated by excluding expansion of cells in each individual division within a given population, that is, dividing cell numbers for cells in division i by 2^i, as described previously (29–32).

Mathematical modeling

The model of proliferation used in this study assumes that cells undergo single stochastic divisions (SSDs) and is therefore termed the SSD model. The model construct is based on one first used by Smith and Martin (SM model) (33) to describe division in cell lines and that has been used more recently in a number of studies quantifying lymphocyte dynamics using CFSE data (28, 34–36). As with the SM model, in the SSD model, cells are in one of two compartments that approximate to resting (A phase) and dividing (B phase) cells (Fig. 1). Cells are assumed to take a fixed time to transit the B phase, corresponding to the G_1, S, G_2, and M phases of the cell cycle. This contrasts with the SM model in which cells in A phase were in G_0 or G_1 arrest, whereas B phase were cells are in S-G_2-M. Furthermore, the SSD model also includes a conditioning time (T) before which cells are not susceptible to induction of homeostatic cell division after transfer. Cells in A phase are considered to be nondividing cells in G_0 state. These cells can then receive a stochastic trigger to enter the cell cycle (B phase) at a rate captured by the parameter, λ. A reduction in λ dependent on the number of cells (competition for resources) was achieved by making $\lambda = \lambda_0 \exp(-\mu N)$, with the parameter μ determining the size of the reduction caused by increasing number of competing cells (N). In this equation, λ_0 can be considered to represent the ability of each clonotype to respond to an unlimited resource (i.e., in the absence of competition), μ can be considered to be proportional to the reciprocal of the resource availability, and N the total number of cells. We assume the impact of T cell number on λ should be proportionally the same for all T cells, regardless of variation in λ_0 values for individual clones. The parameter that quantifies this impact, μ, was therefore made common to both OT-I and F5, and estimated using both data sets together. The B phase, the duration of which is described by the parameter Δ, represents cells in G_1, S, G_2, and M stages of cycle, before returning to G_0. In preliminary model fits, the rate of cell death δ was very close to 0 for both OT-I and F5, suggesting little cell death occurred during the lymphopenia-induced proliferation (LIP) response. Absence of cell death was also evident experimentally by the constant number of T cell precursor numbers observed over time (Fig. 2B). We therefore omitted δ as a model parameter.

SSD model

The SSD model is an adaptation of the SM model (33) as applied previously (28). It is supposed that cells are either in A or B phase (Fig. 1). The time spent in A phase is exponentially distributed, such that each cell can make the A→B transition at a rate λ (the mean time for cells residing in A phase is 1/λ). On entering B phase, each cell undergoes cell division over a fixed time Δ_{TC}. We denote the number of cells having i divisions at time t in A and B phase as $A_i(t)$ and $B_i(t)$, respectively. The population density of cells in B phase will be $b_i(t; s)$, where $s \in [0; \Delta_{TC}]$ is the time spent in B phase. Cells can die in A or B phase at a rate δ. Then the number of cells having undergone a given number of divisions with no death can be calculated recurrently with the separate differential equations (n is the maximum number of divisions that can be distinguished experimentally):

$$\dot{A}_0(t) = -(\lambda+\delta)A_0(t)\{A_0(T) = N_0\}$$

$$\dot{A}_i(t) = 2b_{i-1}(t,\Delta_{TC}) - (\lambda+\delta)A_i(t), \{A_i(T) = 0\}, i = 1\ldots n, t>T$$

$$\frac{\partial b_i(t,s)}{\partial t} + \frac{\partial b_i(t,s)}{\partial s} = -\delta\ b_i(t,s), \{b_i(T,s) = 0, b_i(t,0) = \lambda A_i(t)\}$$

$$B_i(t) = \int_0^{\Delta_{Tc}} b_i(t,s)ds.$$

The total number of cells with a given number i of divisions is $N_i(t) = A_i(t) + B_i(t)$, and the number of precursors is $\gamma_i(t) = 2^{-i}N_i(t)$, leading to the frequency:

$$p_i(t) = \frac{\gamma_i(t)}{\sum_{i=0}^{n}\gamma_i(t)}.$$

When using Ki67 or 7AAD as a cell-cycle marker, we assume that Ki67$^+$ or 7AAD$^+$ cells are in B phase. The predicted frequency of these cells is:

$$\nu_i(t) = \frac{B_i(t)}{A_i(t)+B_i(t)}.$$

In the SSD model, the A→B transition was allowed to decline as a function of total number of cells: $\lambda(N) = \lambda_0 \exp\left(-\eta\sum_{i=0}^{n}N_i(t)\right)$.

The autopilot model

The autopilot model (Supplemental Fig. 1) is similar to models used previously to successfully analyze cell division in response to antigenic stimuli (31). In this model, cells all receive an initial trigger to divide and after a fixed time (T) enter cell division asynchronously with a defined time/frequency distribution. In contrast with the SSD model, once division is initiated, cells continue to divide in a deterministic manner for a fixed number of divisions with cell division times of identical duration (Δ). Modifications of this model allow loss (cell death) during proliferation, but this was not used in this study because no death was detected experimentally over the first 12 d (10–12 divisions) of the response.

This model assumes that all divisions except the first one occur in equal fixed periods of time Δ_{AD}. The time to first division is distributed according to the continuous probability density function Φ(α, β; t). We investigated Weibull, γ, normal, and lognormal distributions. After the delay T of triggering for division, the frequency of cells with i divisions at time t can be calculated by

$$p_{i=0}\left(\vec{\theta},t\right) = 1 - \int_0^{t-T}\Phi(\alpha,\beta;s)ds$$

$$p_{i>0}\left(\vec{\theta},t\right) = \int_{t-T-i\Delta_{AD}}^{t-T-(i-1)\Delta_{AD}}\Phi(\alpha,\beta;s)ds.$$

Parameter estimation

The equations to predict precursor frequencies $p_i(\vec{\theta},t)$ were solved numerically using Runge–Kutta fourth order method. The parameters to estimate were for the two-compartment model: $\vec{\theta} = [\lambda_0, \Delta_{TC}, T, \delta, \mu,\ or\ \eta]$ and for the autopilot model: $\vec{\theta} = [\alpha, \beta, \Delta_{AD}, T]$. We used weighted sums of squared residuals (SSRs) for optimization with variance over observed frequencies with given i at given day as the measurement error function. Minimization with respect to the parameters was done using MatLab v7.11.0 (R2010b; The MathWorks) with the *fminsearch* function.

Comparison of the models

Comparison of the different models was done using a cross-validation approach. The whole data set was separated into two parts: a validation

set with data for one given mouse, m, and a training set with the remaining data (including M-1 mouse).

Parameter values were obtained by minimizing the SSR with the training set. When using CFSE only:

$$SSR_{cfse}^{-m} = \sum_{i=0}^{n}\sum_{k=1}^{K}\sum_{\substack{j=1\\ j\neq m}}^{M} \frac{\left(f_{ij}^{cfse}(t_k) - p_i\left(\overrightarrow{\theta}^{-m}, t_k\right)\right)^2}{\sigma^2_{cfse_i}(t_k)}.$$

And when using CFSE and another marker (either Ki67$^+$ or 7AAD):

$$SSR_{cfse+\text{marker}}^{-\text{m}} = \sum_{i=0}^{n}\sum_{k=1}^{K}\sum_{\substack{j=1\\ j\neq m}}^{M} \frac{\left(f_{ij}^{cfse}(t_k) - p_i\left(\overrightarrow{\theta}^{-m}, t_k\right)\right)^2}{\sigma^2_{cfse_i}(t_k)} + \frac{\left(f_{ij}^{\text{marker}}(t_k) - \nu_i\left(\overrightarrow{\theta}^{-m}, t_k\right)\right)^2}{\sigma^2_{\text{marker}_i}(t_k)},$$

where $f(t)$ and $\sigma^2(t)$ are the observed frequencies and variances, respectively. Here, i stands for the number of divisions (with total number $n = 8$), k is the number of the sampling day (with total number $K = 8$), j is the number of mouse, M is the total number of mice in the experiment ($M = 32$ for OT-I cells and $M = 31$ for F5).

At the next step, for each mouse m, the comparison reference value (CrV) criterion is calculated with the estimated parameter values $\overrightarrow{\theta}*$ using the validation set

$$CrV_m^{cfse} = \sum_{i=0}^{n}\sum_{k=1}^{K} \frac{\left(f_{im}^{cfse}(t_k) - p_i\left(\overrightarrow{\theta}^{-m}, t_k\right)\right)^2}{\sigma^2_{cfse_i}(t_k)}$$

for CFSE only or

$$CrV_m^{cfse+\text{marker}} = \sum_{i=0}^{n}\sum_{k=1}^{K} \frac{\left(f_{im}^{cfse}(t_k) - p_i\left(\overrightarrow{\theta}^{-m}, t_k\right)\right)^2}{\sigma^2_{cfse_i}(t_k)} + \frac{\left(f_{im}^{\text{marker}}(t_k) - \nu_i\left(\overrightarrow{\theta}^{-m}, t_k\right)\right)^2}{\sigma^2_{\text{marker}_i}(t_k)}$$

for CFSE and the additional marker.

The CrV_m and $\overrightarrow{\theta}^{-m}$ were calculated for each experimental mouse m in the validation set. The final estimate of the cross-validation criteria was: $CrV = \frac{1}{M}\sum_{m=1}^{M} CrV_m$. The lower value of CrV indicates the better model.

Results

Contrasting homeostatic responses by F5 and OT-I TCR transgenic T cells

Homeostatic responses of two different TCR clonotypes (OT-I and F5) were analyzed. T cells from F5 TCR transgenic mice are specific for influenza NP (37). They undergo a relatively slow rate of LIP and remain naive in phenotype (26). In contrast, OVA peptide–specific T cells from OT-I TCR transgenic mice undergo much more rapid LIP that is also associated with development of effector function, memory phenotype, and gene expression in vivo (18, 19). The differences in the behavior of these two clones is likely to reflect differences in the functional avidity of each TCR for spMHC and/or differing expression of IL-7R (38, 39), both critical determinants of the LIP response. The broad range of proliferative activity observed when F5 and OT-I T cells undergo LIP mirrors very well that range of responses observed when polyclonal CD8 T cells undergo LIP (28, 40), making these two clones ideal for this study.

Detailed time courses of LIP by both TCR transgenic strains were generated to test the fits of mathematical models (Fig. 1).

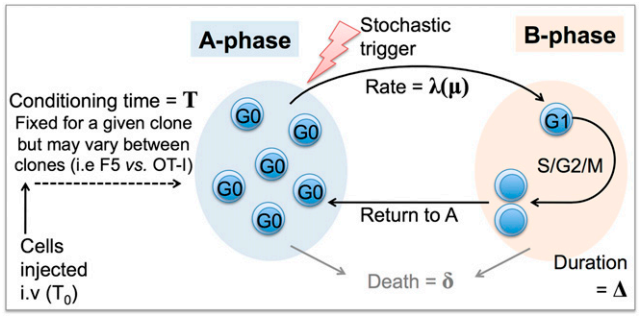

FIGURE 1. SSD model of T cell proliferation. The SSD model of cell division is a modification of an SM (33)–based model described by Yates et al. (28). After injection, cells are subject to a conditioning time (T) before entering A phase, in which they are able to receive a stochastic trigger to divide. Cells that receive this trigger undergo one round of cell cycle in B phase of duration Δ hours, before returning to A phase where they must reaudition for subsequent divisions, regardless of division history. The rate of entry into division (λ) is described by a function of the parameter μ, which is linked to time or to cell number. A rate of death is defined by δ.

After transfer to lymphopenic *Rag1*$^{-/-}$ recipient mice, dye labeling and CD44 expression levels revealed distinct kinetics of proliferation and differentiation (Fig. 2A). Although recoveries of total T cells in both cases increased with time, OT-I cells accumulated in greater numbers consistent with their greater cell division (Fig. 2B). The size of the precursor population of T cells was calculated by excluding the expansive effects of cell division (see *Materials and Methods*). Any reduction in the size of this population would represent a loss of cells, most likely through death or altered homing. The size of the precursor population, however, remained relatively constant over time for both F5 and OT-I T cells (Fig. 2B), indicating that there was little detectable cell death during the course of the experiment.

LIP responses of both F5 and OT-I are accurately captured by the single division competition model

LIP responses of OT-I and F5 were fitted to a density-dependent model of T cell division, which assumes cells undergo SSDs and in which the rate of entry into cell cycle decreases exponentially with increasing cell numbers (Fig. 1). This model, termed SSD hereon, is an adaptation of a previous two-compartment model described and used by SM model to study cell division by cell lines in vitro (33) and applied by us previously to analyze LIP by F5 T cells (28). The SSD model implemented in this study specifically differs from the SM model and its later applications by using a density-dependent rate of cell division and by defining nondividing cells as those specifically in G_0, whereas dividing cells are considered those in G_1-S-G_2-M stages. Best-fit parameters for the SSD model were determined by minimizing weighted SSR for LIP by both F5 and OT-I cells (Table I). As expected from previous studies, the SSD model was successful in describing LIP by F5 T cells as apparent in the predicted division profiles (Fig. 3A) and time course of mean divisions of the populations (Fig. 3B), which in both cases closely matched observed data. Despite the differences between the parameterization of the SSD model and the earlier SM model (28) and the constraining data sets, specific estimates of T, Δ, and λ_0 (2.6, 0.24, and 0.29, respectively) were in close agreement with this earlier study (2.4, 0.26, and 0.45, respectively). Importantly, the SSD model was also successful in describing LIP by OT-I T cells (Fig. 3). The difference in behavior between the two clones was captured by the SSD model with distinct values for the parameters λ_0 (the rate of

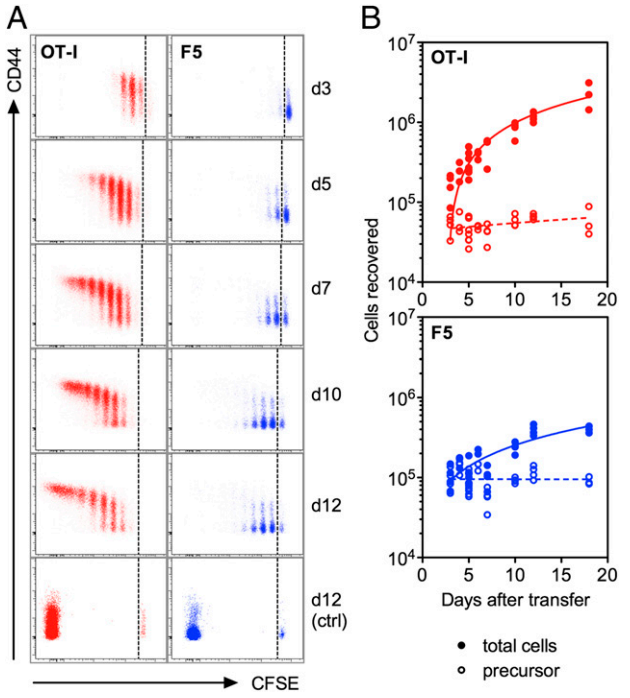

FIGURE 2. Contrasting homeostatic proliferative responses by F5 and OT-I T cells. CFSE-labeled OT-I or F5 T cells were transferred to *Rag1*$^{-/-}$ recipients by i.v. injection (1.5×10^6 cells/mouse). At the indicated days after transfer, spleens and lymph nodes were recovered from recipient mice (n = 3–5 per time point) and analyzed by flow cytometry for expression of CD8, CD5, CD44, and CFSE dilution. (**A**) Representative dot plots gated on CD5$^+$CD8$^+$ lymphocytes show CD44 expression versus CFSE labeling in the lymph nodes of mice that received either OT-I (*left panels*) or F5 cells (*right panels*). (**B**) The recovery of total (closed symbols, solid lines) and precursor (open symbols, dashed lines) cells in recipient mice was calculated from the spleen and lymph nodes. Data are pooled from two independent experiments; lines of best fit were calculated by linear regression, and symbols represent individual mice. Linear regression fits to precursor pool size with time returned no negative slope.

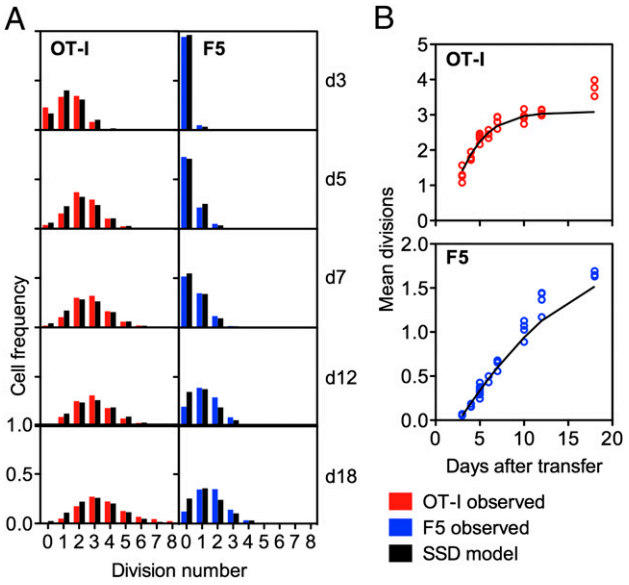

FIGURE 3. Comparison of observed and model-predicted T cell proliferation. Best-fit parameter estimates from the SSD model of cell division were used to predict (**A**) the frequency of precursor cells in each division or (**B**) the mean number of divisions undergone by the donor cell population. At the indicated time points posttransfer, data predicted by the SSD model (black bars, solid black lines) were compared with experimental data for both OT-I (red bars, open red circles) and F5 (blue bars, open blue circles) T cells.

entry into cell division under conditions of unlimited resource availability) and T (the time to first division; Table I). The estimated value of λ_0 was higher for OT-I T cells, consistent with the more rapid response by this clonotype. In contrast, the conditioning time T was shorter for OT-I than F5 T cells. The other key parameter Δ (the duration of cell division) was similar for both F5 (0.24 d) and OT-I (0.34 d) T cells.

Autopilot models based on deterministic cell division processes have proved useful and effective at describing proliferation induced by antigenic stimulation (31). We previously showed that an autopilot model (see Supplemental Fig. 1) was not so suitable for describing F5 LIP data (28). OT-I cells, however, proliferate much more rapidly than F5 in LIP conditions and also acquire a memory phenotype (Fig. 2), suggesting that LIP of OT-I cells may more closely resemble Ag-driven responses. It was therefore important to compare the SSD model with the autopilot model for OT-I, as well as F5. However, it was clear that LIP by OT-I was much better modeled with the SSD model than the "autopilot" model, as reflected in the lower CrV for the SSD model fit, which is a measure of goodness of fit (low is better). This suggests that LIP is more stochastic than deterministic in nature and supported the suitability of the SSD model for both clonotypes (Fig. 4, Table II).

Validating model predictions of T cell behavior

Parameter estimates for the time in cell division (Δ) were 0.34 d (8.16 h) for OT-I and 0.24 d (5.76 h) for F5 (Table I). These values were compared with experimental estimates of duration of the first cell division. Frequency–time distributions for entry of cells into G_1 phase of cycle, identified by Ki67 expression (41), and the distribution of cells completing this first division, identified by analyzing cell dye levels, were determined. The x-axis displacement between these frequency distributions provided an empirical estimate of duration of first cell division (Fig. 5A), taken when half the population had undergone first division. For both F5 and OT-I T cells, Ki67 induction preceded completion of first division by ~8 h, a duration very close to the parameter values estimated by the SSD model (Table I).

Table I. Best-fit parameter estimations for the SSD model

Data	Division History		Division History + Cell Cycle	
Parameters	F5	OT-I	F5	OT-I
λ_0 (/cell/day)	0.29 (0.27–0.47)	1.4 (1.3–1.8)	0.33 (0.26–0.36)	2.1 (1.6–3.0)
Δ (d)	0.24 (0.17–0.73)	0.34 (0.20–0.75)	0.21 (0.14–0.34)	0.28 (0.26–0.36)
T (d)	2.6 (2.4–2.6)	0.72 (0–0.76)	2.5 (2.4–2.6)	1.4 (1.2–2.5)
μ	5.5E-6 (4.9E-6, 6.5E-6)		6.0E-6 (5.2E-6, 7.9E-6)	

Best-fit parameter estimations for the SSD model (Fig. 2) were calculated using cell dye data or cell dye data in combination with cell-cycle information (Fig. 1, Supplemental Figs. 2, 6). Numbers in parentheses are 95% confidence intervals.

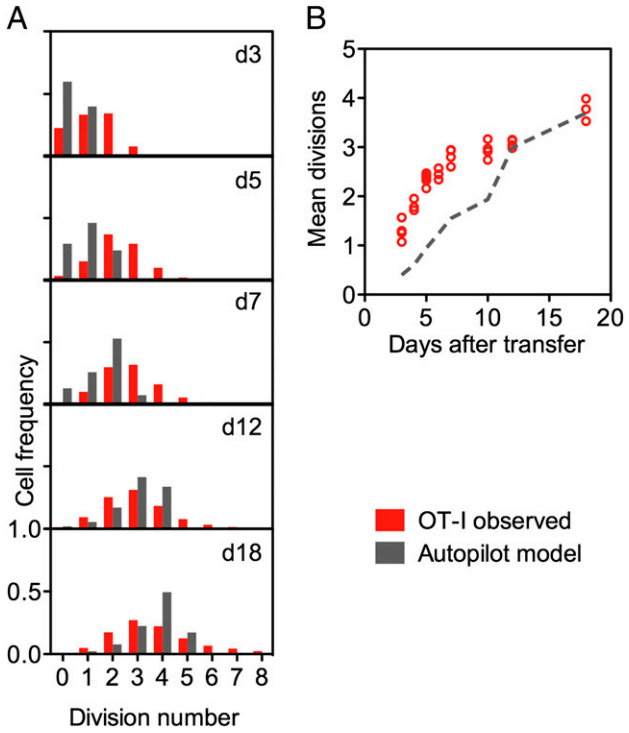

FIGURE 4. Autopilot model does not fit proliferation of OT-I cells. Best-fit parameter estimates from the autopilot model of cell division (see Table II and Supplemental Material) were used to predict (**A**) the frequency of precursor cells in each division or (**B**) the mean number of divisions undergone by the donor cell population. At the indicated time points after transfer, data predicted by the autopilot model (gray) were compared with experimental data for OT-I cells (red).

We next examined the number of divisions triggered during LIP. The model assumes that entry into cell division is cell density dependent (exponentially decreased with increasing cell numbers), and that there is only one cell division before returning to the "resting" A phase. Consistent with these assumptions, LIP of F5 T cells is rapidly halted after quenching lymphopenia by injecting mice with a high dose of T cells (28). Significantly, despite the greater rate of division of OT-I T cells, treatment with WT cells at day 3.5 after initiation of LIP brought about an identical cessation of OT-I and F5 T cell division by day 5 (Fig. 5B), suggesting that continued division was dependent on the lymphopenic state of the host. Simulating the reversal of lymphopenia by increasing N by 10^8 at t = 3.5 d in the SSD model predicted a rapid reduction in T cell proliferation as observed experimentally (Fig. 5B). Therefore, the SSD model can successfully relate T cell division to the host compartment size.

Table II. Parameter estimates for OT-I LIP by the autopilot model compared with the SSD model

Autopilot Model		Two-Compartment (SSD) Model	
Parameters	OT-I	Parameters	OT-I
α	1.25	λ_0 (/cell/day)	2.315
β	3.41	μ	0.41
Δ (d)	2.77	Δ (d)	0.62
T (d)	0.0	T (d)	0.591
CrV	1391	CrV	45.8

Best-fit parameter estimations for the SSD model and the autopilot model for OT-I cells were calculated using cell dye data (fits shown in Fig. 4). For the SSD model, λ_0 is rate of entry into B phase at $n = 0$ where N is the total number of T cells, μ is rate of change in λ with N. For the autopilot model, α and β are parameters for the probability of entry into cell cycle (see Supplemental Material).

Δ, Duration of cell division in both models; T, time before onset of LIP.

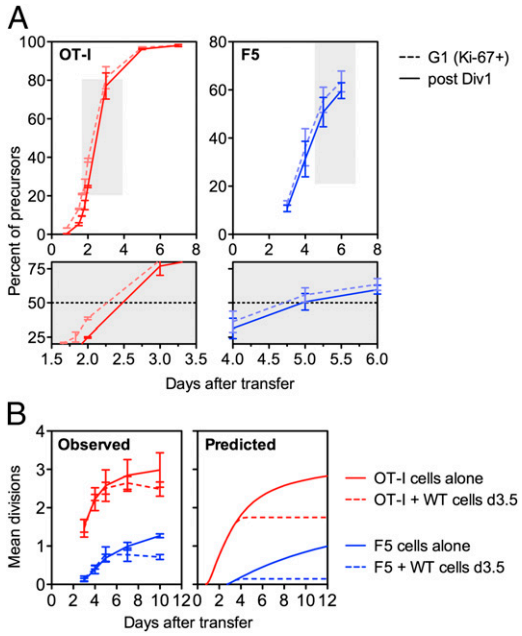

FIGURE 5. Experimental validation of model predictions. (**A**) CFSE-labeled OT-I or F5 T cells were transferred to *Rag1*$^{-/-}$ recipients by i.v. injection (1.5×10^6 cells/mouse). Mice were sacrificed at the indicated days after transfer, and lymph node cells were analyzed by flow cytometry for expression of CD5, CD8, Ki67, and CFSE dilution. Graphs show the frequency–time distribution of OT-I (red) or F5 (blue) precursor cells entering first cell cycle, identified as Ki67$^+$ division 0 (dotted lines; Ki67$^+$ cells), and distribution of cells completing their first division identified by cell dye labeling (solid lines). Mean and SD of at least three mice per group are shown; data are representative of four independent experiments. The cell-cycle time for the first cell division was estimated at the midpoint (*lower panels*, magnified view). (**B**) CFSE-labeled OT-I or F5 T cells were transferred to *Rag1*$^{-/-}$ recipients by i.v. injection (1.5×10^6 cells/mouse). At day 3.5 after transfer, groups of mice either received ~50×10^6 Ly5.1$^+$ WT T cells (dotted lines) or no cells as control (solid lines). At the indicated days after transfer, blood was analyzed by flow cytometry for expression of CD5, CD8, Ly5.2, and CFSE dilution. Mean and SD of five mice per group are shown, and data are representative of two independent experiments. Observed experimental results (*left panel*) were compared with predicted results according to the best-fit parameter values of the SSD model (*right panel*).

Improved parameter estimates using 7AAD as a marker for dividing cells

In the SSD model with two separate compartments for resting and dividing cells, better parameter estimates should be possible if cell numbers in each of the two compartments could be estimated independently. Initial experiments using Ki67 to identify dividing cells proved unsuccessful. We found that Ki67 expression was still detectable in transferred T cells 7 d after lymphopenia was reversed (Fig. 5B, Supplemental Fig. 2). In contrast, the DNA stain 7AAD proved to work well by identifying dividing cells (Fig. 6). The SSD model was therefore constrained using 7AAD to identify dividing cells (Table I). The parameter estimates using 7AAD to estimate dividing cells were very similar to those obtained using total cell numbers only: the main differences being closer estimates of cell-cycle time (Δ) for OT-I and F5 (0.28 and 0.21, respectively) with smaller confidence limits, a slightly longer conditioning time (T) for OT-I (1.4 compared with 0.72 d), and a slightly faster initial rate of entry into cell cycle (λ_0) for OT-I (2.1 compared with 1.2).

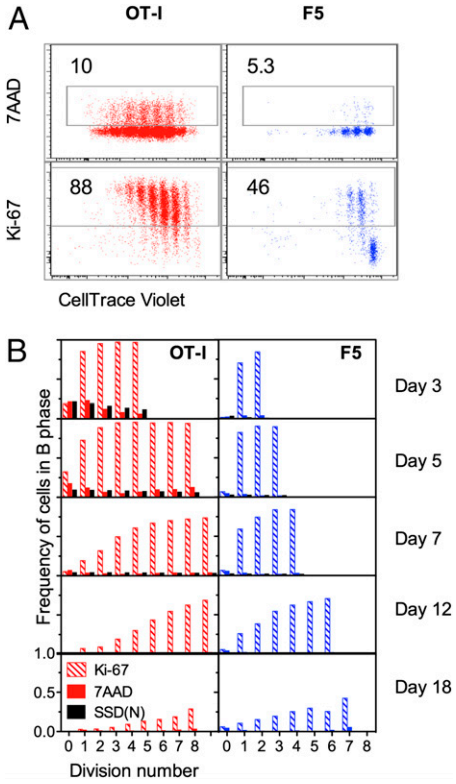

FIGURE 6. Comparison of Ki67 expression and DNA content in T cells with SSD model predictions of cells in B phase. (**A**) CTV-labeled OT-I or F5 T cells were transferred to *Rag1*$^{-/-}$ recipients by i.v. injection (1.5×10^6 cells/mouse). Recipient mice were sacrificed at days 3–18 after transfer, and cells from the spleen and lymph nodes were analyzed by flow cytometry for expression of CD5, CD8, and CTV dilution, as well as either DNA content (by 7AAD stain) or Ki67 expression. Representative dot plots are gated on CD5$^+$CD8$^+$ cells in the lymph nodes of recipient mice at day 5 after transfer. Numbers indicate the frequency of total cells that are actively dividing, defined by either expression of Ki67 or DNA content of >2 N. (**B**) The observed frequency of actively dividing cells according to either Ki67 expression (hatched bars) or DNA content >2 N (solid colored bars) was determined for each division at the days indicated after transfer for both OT-I (red) and F5 (blue) cells. Black bars indicate the predicted frequency of cells in B phase according to the best-fit parameter values of the SSD model (Fig. 1).

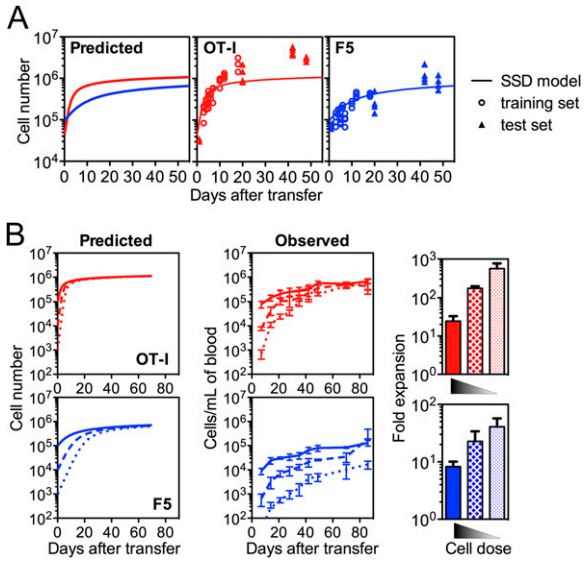

FIGURE 7. SSD model is sensitive to cell density and predicts the dose-dependent expansion of clonal populations. Cell dye data were used to calculate best-fit parameter estimations for the SSD model using training data (Fig. 1). (**A**) Model parameters were then used to predict the total number of F5 or OT-I donor cells in recipient mice at days 1–50 after transfer. Independently, a second set of test data were generated by transferring 1.5×10^6 F5 or OT-I T cells and assessing cell recoveries at days 1, 20, 42, and 48 after transfer. Graphs show predicted expansion of F5 (blue lines) and OT-I (red lines) T cells with observed training data (open circles) and test data (filled triangles) for both OT-I (red) and F5 cells (blue). (**B**) Model parameters were used to predict T cell expansion from different starting cell doses of either 10^3 (dotted lines), 10^4 (long dashed lines), or 10^5 (solid lines). Observed data (*middle* and *right panels*) were generated by sampling blood from the tail vein of mice that received either 2×10^4 (dotted lines), 2×10^5 (long dashed lines), or 2×10^6 (solid lines) donor OT-I or F5 T cells. Recipient mice were sacrificed 1 and 86 d after transfer, and total F5 and OT-I T cell numbers in the spleen and lymph node were calculated. Bar charts show fold expansion of F5 and OT-I T cells at day 86 over initial engraftment at day 1. Data are representative of two independent experiments with at least four mice per group.

Predicting the kinetics and duration of LIP

The SSD model provided detailed and accurate descriptions of cell-cycle behavior and cell division dynamics. However, a sterner test would be to determine whether the model could predict the timing and magnitude of the homeostatic point of equilibrium (the set point). For this, we used the best-fit parameters obtained using 7AAD to identify dividing cells. The SSD model predicted that F5 and OT-I LIP would reach distinct set points, higher for OT-I than for F5 (Fig. 7). These predictions were then compared with the original training data set and a test data set generated to specifically measure the T cell population expansion at later time points, beyond those used for the training data set. For F5 T cells, the model provided good fits of the training data and made remarkably good predictions of continued cell expansion close to that observed in the test experimental data set (Fig. 7A). Predicted expansion of OT-I T cells was reasonable over the range of the training data set (Fig. 7A), but the observed homeostatic set point measured in the test data set was ~2- to 4-fold greater than the model prediction. Of significance, however, was that test data clearly showed that the set point for OT-I T cells (4×10^6) is ~4-fold greater than for F5 T cells (~1×10^6). This difference in set point for the two T cell clones shown experimentally was successfully captured by the model (Fig. 7A).

To further test the effect of cell number, we used the model to predict growth of T cell populations using different initial starting cell numbers. In each case, the model predicted a convergence of T cell expansion to a common set point, regardless of starting N (Fig. 7B). This was expected as the model has only one steady-state. Three doses of F5 or OT-I T cells were transferred to *Rag1*$^{-/-}$ recipients and T cell number in blood followed over time to determine whether this was also observed experimentally. For OT-I, all three doses converged on a common set point (Fig. 7B). For F5 T cells, both higher doses converged on a similar set point, whereas the lowest dose had not yet reached the plateau achieved by the higher doses (Fig. 7B). However, analysis of total T cell numbers in cohorts of mice at day 1 and the experiment end at day 86 revealed extensive T cell expansion in all transfers (Fig. 7B). The fold expansion was inversely proportional to inoculating cell dose and was greatest for the lowest initial starting cell number for both clones (Fig. 7B). In the case of the lowest F5 T cell dose, cells had expanded 40 times, the most of the 3 doses, and total recoveries were only 2–5 times less than the other higher doses. Therefore, the expected behavior of the SSD model, having a single set point regardless of starting dose, was for the most part reflected by the LIP response of OT-I and F5 T cells.

Clonal competition between OT-I and F5

The SSD mathematical model described in this article is based on competition between T cells for a resource required for homeostatic proliferation where the rate of entry into cell division λ decreases with increasing cell numbers and/or decreasing availability of the resource. One important question that arises from such a model is whether different clonotypes, in this case, OT-I and F5, compete for the same resource (such as IL-7) or a different resource, which could, for example, be spMHC. If OT-I and F5 compete for the same resource, the SSD model will give different trajectories of cell numbers over time for LIP with both clonotypes combined compared with individual OT-I and F5 responses. To examine this, we determined the predicted trajectories for OT-I and F5 alone and in combination, with the tacit assumption of the model of competition for the same resource (Fig. 8A). The presence of competing F5 cells had a small impact on predicted OT-I cell expansion. In contrast, expansion of F5 cells was substantially reduced by the presence of competing OT-I cells. These different effects can be explained by the lower value of λ_0 for F5 compared with OT-I (0.33 compared with 2.1 as shown in Table I). Because λ_0 is the maximum rate of division in the absence of competition, this parameter could also reflect the ability of each clonotype to compete for a common resource. LIP in mice reconstituted with OT-I and F5 either alone or in combination was determined experimentally to confirm these model predictions (Fig. 8B). The results from this experiment are remarkably similar to the model predictions, strongly supporting competition between OT-I and F5 for the same resource.

Discussion

After activation by Ag, T cells are triggered into a rapid burst of ~10–15 cell divisions resulting in profound expansion (42). Cell division can occur extremely rapidly, as fast as 2–3 h (43), and independently of further TCR triggering, at least to some extent (44). In contrast, homeostatic cell division is characterized by a slower rate and fewer divisions. This generalized view is complicated, however, by substantial heterogeneity in homeostatic responses in terms of whether to divide, and if so, how fast to divide, and whether division is accompanied by differentiation into memory-like cells. It has been unclear whether such diverse behavior is governed by a set of rules common to all T cells and whether these rules were fundamentally the same or different from those of Ag-induced proliferation. In this study, we found that diverse clonal responses of naive T cells to lymphopenia in mice can be accounted for by a common model of cell-cycle control based on SSDs with resource competition between T cells. LIP of OT-I T cells is among the most rapid reported for any class I–restricted TCR transgenic (25) and was estimated here to be five to seven times the rate of F5 T cells. Despite this, an autopilot model of cell division was less effective at describing OT-I T cell LIP. In addition, OT-I T cell proliferation was halted by reversal of lymphopenia in an identical manner to F5 T cells, despite the substantial differences in proliferation rate, showing that continued lymphopenia for both OT-I and F5 T cells was required for LIP. This finding is inconsistent with autopilot models that require only an initial triggering stimulus. Taken together, these results strongly suggest that the two T clonotypes are controlled by the same qualitative mechanisms and in a similar manner.

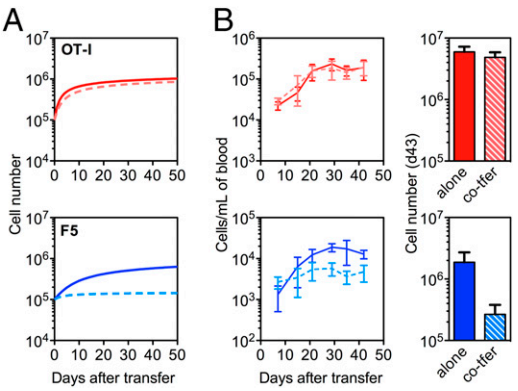

FIGURE 8. Competition between OT-I and F5 cells. Cell dye data were used to calculate best-fit parameter estimations for the SSD model using training data (Fig. 1). (**A**) Model parameters were then used to predict the total number of F5 (blue) or OT-I (red) donor cells in recipient mice at days 1–50 after transfer. Predictions were made for OT-1 and F5 cells transferred alone (solid line) or combined (dotted line). (**B**) CFSE-labeled OT-I and/or F5 T cells were transferred to *Rag1*$^{-/-}$ recipients by i.v. injection either independently (10^6 cells/mouse) or together (10^6 cells of each clonotype per mouse). Blood was sampled from the tail vein of recipient mice at weekly intervals and numbers of transferred populations of T cells calculated (*left panel*) for OT-I or F5 T cells transferred either independently (solid lines) or together (dotted lines). Recipient mice were sacrificed at 43 d after transfer, and total donor T cell numbers in the spleen and lymph node were calculated. Bar charts show total OT-I (red) or F5 (blue) cells recovered from mice that received either a single clonotype (solid bars) or both clonotypes (striped bars). Mean and SD of at least five mice per group are shown.

Analyzing the diverse proliferative responses of OT-I and F5 T cells with the SSD model helped identify those key parameters that define clonal homeostatic reactivity. The duration of cell division during LIP (Δ) identified from best-fit parameter estimations revealed division times of between 5 and 7 h (Table I) that were approximately the same for both T cell clonotypes. Empirical measurements confirmed the accuracy of these estimates and together suggest that the time taken to progress through the cell cycle is independent of TCR specificity. In contrast, the rate of entry into cell division in the absence of any T cell competition (λ_0) represented a key and independent clonal property. There was ~6-fold difference in λ_0 between OT-I and F5 T cells (Table I). In addition to distinct functional avidities for spMHC, F5 and OT-I T cells also express different levels of IL-7Rα (38). IL-7 induces cell growth in T cells (45), and this is required for TCR-triggered LIP responses (13). Therefore, higher IL-7Rα expression may account for faster rate of entry into cell division of OT-I cells. Another parameter that was distinct between OT-I and F5 cells was the time to initiation of LIP (T). Both T cells required time in which to "detect" lymphopenia after transfer and to respond, but this was somewhat shorter for OT-I T cells than F5 cells (1.4 versus 2.5 d). However, the clonotypic differences in T (time to first division) were modest next to a time scale of weeks for the proliferative response and have a minor impact on predictions of LIP. Thus, the parameter λ_0 likely represents the key clonotypic property defining the differences in homeostatic behavior of different T cells, and other parameters (T, Δ, μ) share similar or identical values between clonotypes.

Constraining the model further by including cell-cycle data obtained by measuring DNA content with 7AAD provided modest improvements in accuracy of parameter estimations (Table I). DNA staining provided measurements of cells in cycle remarkably close to the estimations for cells in B phase obtained from the models. In contrast, induction of Ki67 was only a good predictor of entry of undivided cells into cell cycle, and it appears that cells maintained expression long after completion of division. Our own data from mice in which lymphopenia was reversed showed that Ki67 in vivo has a relatively long $t_{1/2}$ in the absence of continued cell division because Ki67 expression was detectable even 7 d after

reversing lymphopenia (Supplemental Fig. 2). Therefore, Ki67 indicates recent cell-cycle activity rather than being a strict marker of current division. In support of this view, attempts to use Ki67 data to constrain the model were unsuccessful. However, these data did reveal many Ki67 negative cells in all divisions, including division 1, at 10 d after cell transfer. This clearly indicates that cells do ultimately return to a G_0 state, and for cells in division 1, this is clearly after just a single division.

The finding that a single model can account for the diverse behavior of two distinct T cell clones greatly increases the prospect that homeostasis of the T cell compartment can be successfully and usefully modeled in the future. The two-compartment SSD models used in this study were successful in capturing the finer details of the LIP of both clones and, perhaps most significantly, in predicting set points for each. Identifying λ_0 as the key clonotype-specific parameter should help construct simple models. Significant challenges remain. The distribution of λ_0 in the CD8 repertoire is not known. In addition, cell death did not play a significant role in LIP over the first 20 d of the response and was convenient to ignore. However, it is extremely unlikely that this will be the case in more complex settings, with mixed populations. Another key issue is the impact of intraclonal and interclonal competition. In this study, we analyzed OT-I and F5 T cell responses in isolation and in competition with each other. The model predictions in this case were remarkably similar to experiment (Fig. 7) and are entirely consistent with interclonal competition for a common resource. One obvious contender is IL-7. In this case, the parameter λ_0 might reasonably be interpreted as the ability of each clonotype to respond to IL-7. This interpretation is consistent with the known higher level of IL-7R expression on OT-I cells compared with F5. In physiological settings, the repertoire consists of many clones. Intraclonal competition can occur at the level of access for specific spMHC, whereas interclonal competition can occur both for cellular access to DCs, which are relatively rare cells in lymph nodes, and competition for soluble homeostatic factors such as IL-7 and other cytokines. The SSD model presented in this article has the potential to take these extra factors into consideration without losing the ability to identify key parameter values, and offers the real prospect of formulating models that can accurately describe and predict behavior of the heterogenous T cell compartment. Such models would represent the genuine prospect of systems level modeling of T cell homeostasis that could test and predict the impact of pharmaceutical or infectious perturbations of different aspects of T cell function.

Acknowledgments

We thank the Biological Services staff for assistance with mouse breeding.

Disclosures

The authors have no financial conflicts of interest.

References

1. Jameson, S. C. 2005. T cell homeostasis: keeping useful T cells alive and live T cells useful. *Semin. Immunol.* 17: 231–237.
2. Freitas, A. A., and B. Rocha. 2000. Population biology of lymphocytes: the flight for survival. *Annu. Rev. Immunol.* 18: 83–111.
3. Seddon, B., and R. Zamoyska. 2002. TCR and IL-7 receptor signals can operate independently or synergize to promote lymphopenia-induced expansion of naive T cells. *J. Immunol.* 169: 3752–3759.
4. Schluns, K. S., W. C. Kieper, S. C. Jameson, and L. Lefrançois. 2000. Interleukin-7 mediates the homeostasis of naïve and memory CD8 T cells in vivo. *Nat. Immunol.* 1: 426–432.
5. Vivien, L., C. Benoist, and D. Mathis. 2001. T lymphocytes need IL-7 but not IL-4 or IL-6 to survive in vivo. *Int. Immunol.* 13: 763–768.
6. Tan, J. T., E. Dudl, E. LeRoy, R. Murray, J. Sprent, K. I. Weinberg, and C. D. Surh. 2001. IL-7 is critical for homeostatic proliferation and survival of naive T cells. *Proc. Natl. Acad. Sci. USA* 98: 8732–8737.
7. Labrecque, N., L. S. Whitfield, R. Obst, C. Waltzinger, C. Benoist, and D. Mathis. 2001. How much TCR does a T cell need? *Immunity* 15: 71–82.
8. Seddon, B., and R. Zamoyska. 2002. TCR signals mediated by Src family kinases are essential for the survival of naive T cells. *J. Immunol.* 169: 2997–3005.
9. Witherden, D., N. van Oers, C. Waltzinger, A. Weiss, C. Benoist, and D. Mathis. 2000. Tetracycline-controllable selection of CD4(+) T cells: half-life and survival signals in the absence of major histocompatibility complex class II molecules. *J. Exp. Med.* 191: 355–364.
10. Kirberg, J., A. Berns, and H. von Boehmer. 1997. Peripheral T cell survival requires continual ligation of the T cell receptor to major histocompatibility complex-encoded molecules. *J. Exp. Med.* 186: 1269–1275.
11. Polic, B., D. Kunkel, A. Scheffold, and K. Rajewsky. 2001. How alpha beta T cells deal with induced TCR alpha ablation. *Proc. Natl. Acad. Sci. USA* 98: 8744–8749.
12. Brocker, T. 1997. Survival of mature CD4 T lymphocytes is dependent on major histocompatibility complex class II-expressing dendritic cells. *J. Exp. Med.* 186: 1223–1232.
13. Saini, M., C. Pearson, and B. Seddon. 2009. Regulation of T cell-dendritic cell interactions by IL-7 governs T-cell activation and homeostasis. *Blood* 113: 5793–5800.
14. Kieper, W. C., J. T. Burghardt, and C. D. Surh. 2004. A role for TCR affinity in regulating naive T cell homeostasis. *J. Immunol.* 172: 40–44.
15. Kieper, W. C., and S. C. Jameson. 1999. Homeostatic expansion and phenotypic conversion of naïve T cells in response to self peptide/MHC ligands. *Proc. Natl. Acad. Sci. USA* 96: 13306–13311.
16. Viret, C., F. S. Wong, and C. A. Janeway, Jr. 1999. Designing and maintaining the mature TCR repertoire: the continuum of self-peptide:self-MHC complex recognition. *Immunity* 10: 559–568.
17. Goldrath, A. W., and M. J. Bevan. 1999. Low-affinity ligands for the TCR drive proliferation of mature CD8+ T cells in lymphopenic hosts. *Immunity* 11: 183–190.
18. Hamilton, S. E., M. C. Wolkers, S. P. Schoenberger, and S. C. Jameson. 2006. The generation of protective memory-like CD8+ T cells during homeostatic proliferation requires CD4+ T cells. *Nat. Immunol.* 7: 475–481.
19. Goldrath, A. W., C. J. Luckey, R. Park, C. Benoist, and D. Mathis. 2004. The molecular program induced in T cells undergoing homeostatic proliferation. *Proc. Natl. Acad. Sci. USA* 101: 16885–16890.
20. Tough, D. F., and J. Sprent. 1994. Turnover of naive- and memory-phenotype T cells. *J. Exp. Med.* 179: 1127–1135.
21. den Braber, I., T. Mugwagwa, N. Vrisekoop, L. Westera, R. Mögling, A. B. de Boer, N. Willems, E. H. R. Schrijver, G. Spierenburg, K. Gaiser, et al. 2012. Maintenance of peripheral naive T cells is sustained by thymus output in mice but not humans. *Immunity* 36: 288–297.
22. Asquith, B., J. A. Borghans, V. V. Ganusov, and D. C. Macallan. 2009. Lymphocyte kinetics in health and disease. *Trends Immunol.* 30: 182–189.
23. Soares, M. V., N. J. Borthwick, M. K. Maini, G. Janossy, M. Salmon, and A. N. Akbar. 1998. IL-7-dependent extrathymic expansion of CD45RA+ T cells enables preservation of a naive repertoire. *J. Immunol.* 161: 5909–5917.
24. Swainson, L., S. Kinet, C. Mongellaz, M. Sourisseau, T. Henriques, and N. Taylor. 2007. IL-7-induced proliferation of recent thymic emigrants requires activation of the PI3K pathway. *Blood* 109: 1034–1042.
25. Ge, Q., A. Bai, B. Jones, H. N. Eisen, and J. Chen. 2004. Competition for self-peptide-MHC complexes and cytokines between naive and memory CD8+ T cells expressing the same or different T cell receptors. *Proc. Natl. Acad. Sci. USA* 101: 3041–3046.
26. Ferreira, C., T. Barthlott, S. Garcia, R. Zamoyska, and B. Stockinger. 2000. Differential survival of naive CD4 and CD8 T cells. *J. Immunol.* 165: 3689–3694.
27. Tanchot, C., F. A. Lemonnier, B. Pérarnau, A. A. Freitas, and B. Rocha. 1997. Differential requirements for survival and proliferation of CD8 naïve or memory T cells. *Science* 276: 2057–2062.
28. Yates, A., M. Saini, A. Mathiot, and B. Seddon. 2008. Mathematical modeling reveals the biological program regulating lymphopenia-induced proliferation. *J. Immunol.* 180: 1414–1422.
29. Lyons, A. B., and C. R. Parish. 1994. Determination of lymphocyte division by flow cytometry. *J. Immunol. Methods* 171: 131–137.
30. Wells, A. D., H. Gudmundsdottir, and L. A. Turka. 1997. Following the fate of individual T cells throughout activation and clonal expansion. Signals from T cell receptor and CD28 differentially regulate the induction and duration of a proliferative response. *J. Clin. Invest.* 100: 3173–3183.
31. Gett, A. V., and P. D. Hodgkin. 2000. A cellular calculus for signal integration by T cells. *Nat. Immunol.* 1: 239–244.
32. Lyons, A. B. 2000. Analysing cell division in vivo and in vitro using flow cytometric measurement of CFSE dye dilution. *J. Immunol. Methods* 243: 147–154.
33. Smith, J. A., and L. Martin. 1973. Do cells cycle? *Proc. Natl. Acad. Sci. USA* 70: 1263–1267.
34. Ganusov, V. V., S. S. Pilyugin, R. J. de Boer, K. Murali-Krishna, R. Ahmed, and R. Antia. 2005. Quantifying cell turnover using CFSE data. *J. Immunol. Methods* 298: 183–200.
35. De Boer, R. J., V. V. Ganusov, D. Milutinović, P. D. Hodgkin, and A. S. Perelson. 2006. Estimating lymphocyte division and death rates from CFSE data. *Bull. Math. Biol.* 68: 1011–1031.
36. Pilyugin, S. S., V. V. Ganusov, K. Murali-Krishna, R. Ahmed, and R. Antia. 2003. The rescaling method for quantifying the turnover of cell populations. *J. Theor. Biol.* 225: 275–283.

37. Mamalaki, C., J. Elliott, T. Norton, N. Yannoutsos, A. R. Townsend, P. Chandler, E. Simpson, and D. Kioussis. 1993. Positive and negative selection in transgenic mice expressing a T-cell receptor specific for influenza nucleoprotein and endogenous superantigen. *Dev. Immunol.* 3: 159–174.
38. Sinclair, C., M. Saini, I. S. van der Loeff, S. Sakaguchi, and B. Seddon. 2011. The long-term survival potential of mature T lymphocytes is programmed during development in the thymus. *Sci. Signal.* 4: ra77.
39. Palmer, M. J., V. S. Mahajan, J. Chen, D. J. Irvine, and D. A. Lauffenburger. 2011. Signaling thresholds govern heterogeneity in IL-7-receptor-mediated responses of naïve CD8(+) T cells. *Immunol. Cell Biol.* 89: 581–594.
40. Ernst, B., D. S. Lee, J. M. Chang, J. Sprent, and C. D. Surh. 1999. The peptide ligands mediating positive selection in the thymus control T cell survival and homeostatic proliferation in the periphery. *Immunity* 11: 173–181.
41. Bruno, S., and Z. Darzynkiewicz. 1992. Cell cycle dependent expression and stability of the nuclear protein detected by Ki-67 antibody in HL-60 cells. *Cell Prolif.* 25: 31–40.
42. Kemp, R. A., T. J. Powell, D. W. Dwyer, and R. W. Dutton. 2004. Cutting edge: regulation of CD8+ T cell effector population size. *J. Immunol.* 173: 2923–2927.
43. Yoon, H., T. S. Kim, and T. J. Braciale. 2010. The cell cycle time of CD8+ T cells responding in vivo is controlled by the type of antigenic stimulus. *PLoS ONE* 5: e15423.
44. Obst, R., H. M. van Santen, D. Mathis, and C. Benoist. 2005. Antigen persistence is required throughout the expansion phase of a CD4(+) T cell response. *J. Exp. Med.* 201: 1555–1565.
45. Rathmell, J. C., E. A. Farkash, W. Gao, and C. B. Thompson. 2001. IL-7 enhances the survival and maintains the size of naive T cells. *J. Immunol.* 167: 6869–6876.